DOI: 10.1002/stco.202200039

Dieter Ungermann, Tim Lemański, Bettina Brune

ARTICLE

A Eurocode-compliant design approach for cold-formed steel sections

A Eurocode-compliant design approach was developed for the design of thin-walled cold-formed steel sections which combines the AISI S100-16-Direct Strength Method (DSM) with the design provisions of EN 1993-1-3. The new design approach transfers the cross-sectional resistance determined acc. to DSM based on numerical elastic buckling analyses on the gross cross-section into the global member verification acc. to EN 1993-1-3. Additional factors were introduced to optimize the new approach, e.g., to account for the effects of the nonlinear stress distribution in cross-sections subject to local and/or distortional buckling. Within the framework of the German research project FOSTA P1328/IGF 19964, an extensive series of tests on differently shaped, perforated, and unperforated cold-formed sections in compression and bending were conducted which serve to analyze the buckling phenomena and the load-bearing capacity and to validate the new design approach. In addition, a numerical model was developed, calibrated to the tests, and used for further parametric analyses on the load-bearing capacity of cold-formed sections.

Keywords cold-formed steel sections; stability; EN 1993-1-3; Direct Strength Method (DSM)

1 Introduction

Thin-walled, cold-formed steel sections are used in a wide range of areas from industrial steel structures to special applications like viticulture. The variety of cross-sectional shapes with or without corrugations, folds, grooves, and stiffeners is large. However, the great advantages of individual design and demand-oriented profiling of cold-formed sections are offset by great difficulties in the realistic theoretical assessment of resistance and serviceability.

In Europe, the design of cold-formed members and sheeting is standardized in EN 1993-1-3:2010 [1] whose basic design provisions were mainly developed for C- and Z-shaped steel sections. For deviation, free cross-sectional shapes, design acc. to EN 1993-1-3 is questionable or only possible to limited extent; for continuously perforated sections, theoretical design acc. to EN 1993-1-3 is even impossible. Furthermore, design provisions of EN 1993-1-3 are complicated. This is first of all due to the complex, also coupled instability modes of cold-formed profiles. However, this is also due to the normative design specification and the prescribed use of the method of effective widths [1]. All in all, a design acc. to EN 1993-1-3 is evaluated as time-consuming, error-prone, and usually provides conservative predictions.

This article presents the research results from the German research project FOSTA P1328/IGF 19964 [2], which led to development and validation of a combined AISI S100-16 DSM/EN 1993-1-3 design approach. With this new design approach, the complicated method of effective widths is omitted, as the cross-sectional resistance is determined by means for user-friendly Direct Strength Method (DSM) acc. to the American standardization AISI [3]. The subsequent design for cross-sections in global or coupled instabilities fallows EN 1993-1-3, but with the inclusion of new adjustment factors, which capture, e.g., the unfavorable influence from the nonlinear stress distribution of cold-formed cross-sections in local and distortional buckling.

In-depth considerations and scientific investigations on the transfer of the American AISI DSM design provisions for the determination of the cross-sectional resistance into the European design approach EN 1993-1-3 had already been presented and intensively discussed in the ECCS Technical Working Group TWG 7.5 chaired by and with contributions of the co-author B. Brune [4–9]. However, the initial research had outlined that unacceptable, nonconservative predictions of the load-bearing capacities for cold-formed sections were obtained with the first, simplified proposals [4–8]. Extensive research was deemed necessary to validate a safe, new design approach based on theoretical analyses, tests, and numerical simulations for a wide range of cold-formed steel sections in various lengths. This led to the research project FOSTA P1328/IGF 19964 [2] initiated by the authors in 2018.

The authors regret that due to the complexity of the research subject and the limited scope of this article, only a summary of the most important results of the research project FOSTA P1328/IGF 19964 [2] can be presented. Therefore, the focus of this article is on the basic derivations and presentation of the new combined design approach, a validation can unfortunately only be done here exemplarily on the basis of selected component tests and numerical simulations. Of course, however, extensive theoretical, experimental, and numerical analyses were conducted in the course of the research project FOSTA

P1328/IGF 19964 [2]. A large number of various perforated and nonperforated C-, Ω-, Z- as well as free shaped cross-sections in different length were investigated to analyze the buckling behavior on a parameter basis and to determine the load-bearing capacity of the sections. For further data and details of the tests conducted, the numerical simulations, the buckling analyses, and the individual components of the combined design approach, reference can therefore only be made to the research report [2] within the scope of this article. For verification and ease for the reader, explicit reference from [2] including relevant page numbers, figures, and tables is inserted in the following article at the appropriate places. This article is an extended version of [10], which was part of the conference SDSS in Portugal 2022.

2 Elastic-critical buckling modes of cold-formed sections in compression

The load-bearing behavior of thin-walled cold-formed steel sections in compression is influenced by local, distortional, and global buckling modes, such as flexural, torsional, and torsional-flexural buckling, and interactive local-distortional-global buckling modes. Exemplarily, the isolated buckling modes of a C-shaped cold-formed section in compression are shown in Fig. 1. The signature curve presents the elastic critical buckling loads as a function of the half-wavelength.

Local buckling will occur if individual thin-walled, plane cross-sectional elements are characterized by a large width-to-thickness ratio. However, a pure local buckling mode can usually not be observed in open, thin-walled cross-sections (just in case of short member length).

Distortional buckling may occur in cold-formed sections with edge or intermediate stiffeners such as lips or beads. These stiffeners serve to stiffen the plane thin-walled cross-sectional elements against local buckling, but they are themselves subject to compressive stresses and therefore, in turn, susceptible to buckling. Distortional buckling can usually be recognized by a “closing” or “opening” of open, edge-stiffened cross-sections.

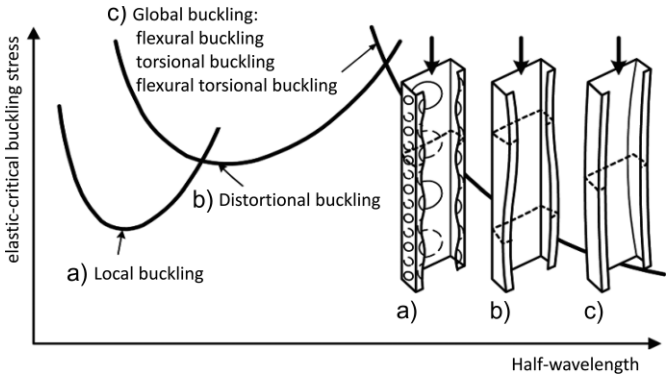

Fig. 1 Elastic-critical buckling modes of thin-walled cold-formed steel sections in compression acc. to EN 1993-1-3 [1]

In the case of global buckling, the cross-section retains its cross-sectional shape and the member in compression may be subject to flexural, torsional, or flexural–torsional buckling. For beams in bending, lateral–torsional buckling becomes relevant.

In practical applications of cold-formed sections, pure buckling modes do not usually occur; rather, local, distortional, and global buckling modes interact. Combined local(-distortional)–global or distortional–global buckling modes are usually observed. However, when analyzing tests and numerical simulations of cold-formed steel components in compression and bending, it is difficult to clearly separate the pure, isolated buckling modes and to capture the different effects from local-(distortional)–global buckling modes on the overall buckling behavior of the cold-formed members (see [2: p. 66–71, 103–104 and clause 5, Tab. 5-3, 5-4]).

3 Standards and design approaches

3.1 EN 1993-1-3 [1]

The European standard approach of EN 1993-1-3 for the design of cold-formed members and sheeting is based on the method of effective widths. For each thin-walled cold-formed cross-section, reduced effective cross-sections shall be determined as a function of loading, capturing the possible unfavorable local and distortional buckling effects on the cross-sectional resistance for that specific type of loading. For cold-formed steel sections, the effective cross-sections are to be determined separately for the basic load cases (A) axial compressive force and (B) bending moments. Fig. 2 shows an overview of the design approach acc. to EN 1993-1-3, 5.5.

According to EN 1993-1-3, the effective widths of the thin-walled plane elements of a cold-formed cross-section accounting for local buckling effects are first determined using the effective width method acc. to EN 1993-1-5 [11]. In the second design step, distortional buckling is considered according to EN 1993-1-3, 5.5.3, which leads to a further reduction of area/thickness of the effective cross-section for the relevant edge or intermediate stiffeners in compression. In summary, the design steps 1 and 2 acc. to EN 1993-1-3 (accounting for local and distortional buckling effects) result in an effective cross-section with a reduced cross-sectional resistance, which serves as the base cross-section for the final design step, i.e., the subsequent global buckling verification of the structural members acc. to EN 1993-1-3, clause 6.2.

In the case of typically open, simply symmetric, cold-formed cross-sections under compressive stress, the center of gravity of the effective cross-section does not usually coincide with the center of gravity of the gross cross-section. Provided that the compressive force still acts axially at the center of gravity of the gross cross-section as planned, the effective cross-section with its changed center of gravity

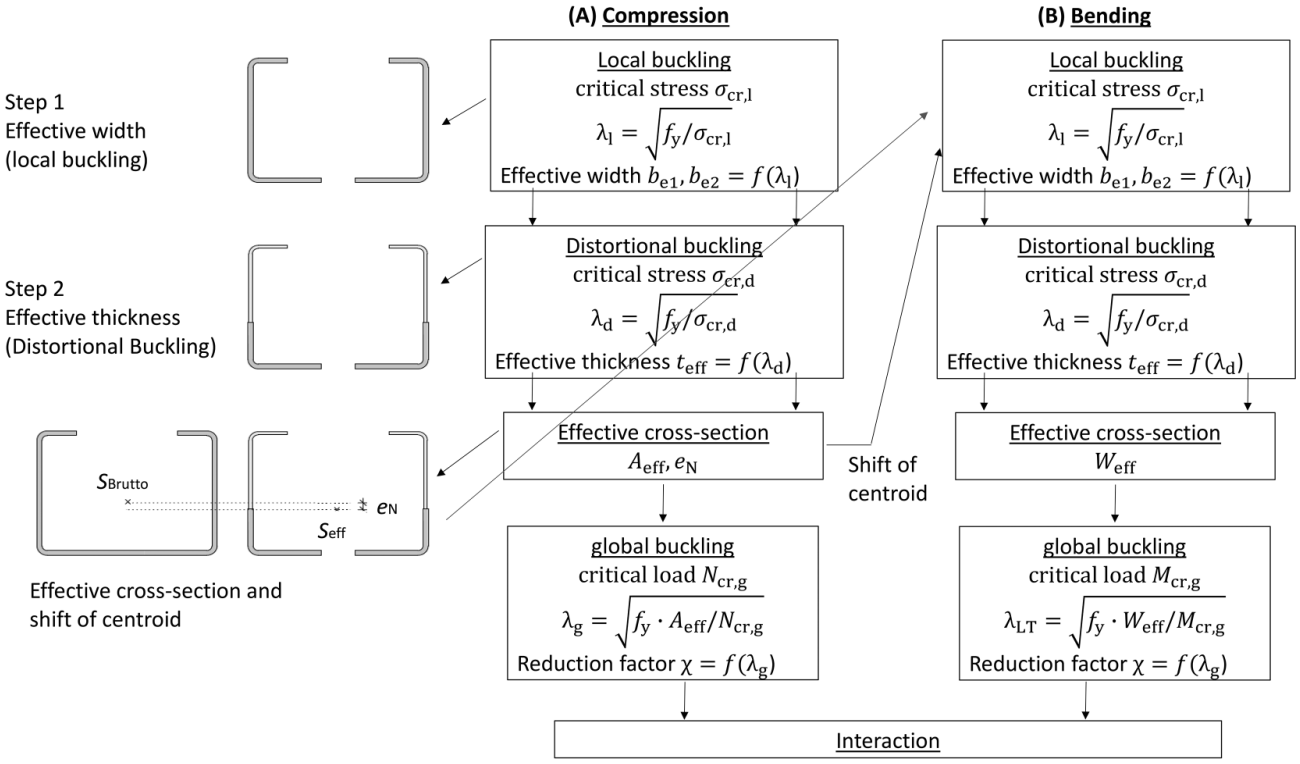

Fig. 2 Flow chart of the design for a C-shaped section in compression acc. to EN 1993-1-3 (notation adjusted for better comparability)

position is now stressed by an eccentric compressive force, so that an additional bending moment $\Delta M = N \cdot e_N$ arises at the effective cross-section. According to EN 1993-1-3, 6.1.3(3), this effect has to be considered by an N–M interaction check both in determining the cross-sectional resistance and in the global stability verification of the member. In this case, an additional effective cross-section loaded by bending stresses has therefore to be determined acc. to EN 1993-1-3, design steps 1 and 2 (Fig. 2, right column).

3.2 DSM according to AISI S100-16 [3]

According to the DSM of AISI S100-16 [3], clause E–G, the cross-sectional and member resistance is always determined on the basis of the gross cross-section, considering all relevant local, distortional, global, or interactive buckling modes. The numerical elastic-critical buckling analysis on the total cross-section is to be conducted first using the freely available finite strip software CUFSM [12], with which the pure buckling modes can be approximately isolated and the phenomenological buckling behavior can be analyzed. However, with finite strip methods (FSM), only cross-sections that remain unchanged along the member length can be modelled in principle which basically limits the use of CUFSM to unperforated sections. Alternatively, finite element (FE) software can be used to determine elastic-critical buckling loads.

In agreement with EN 1993-1-3, the buckling resistance of cold-formed members has to be determined separately for the basic load cases (A) axial compressive force and (B) bending moments. In Fig. 3, the flow chart of an AISI DSM design for members in compression is illustrated.

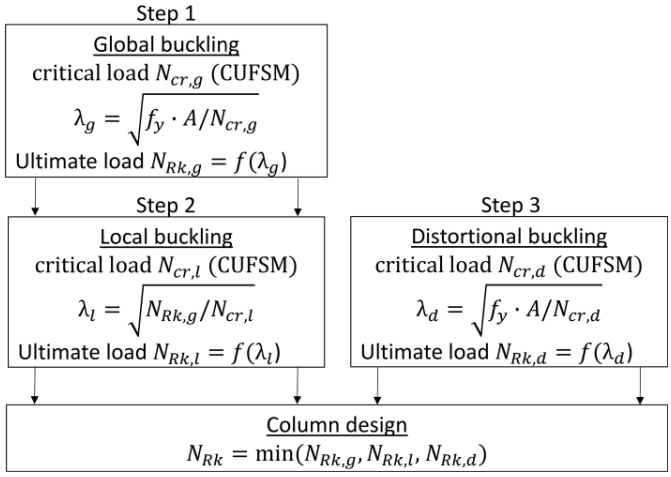

Fig. 3 Flow chart of the design for cold-formed members acc. to AISI S100-16 DSM [3] (notation adjusted for better comparability)

In contrast to EN 1993-1-3, the first design step acc. to AISI DSM is to determine the global buckling resistance of cold-formed members considering flexural, torsional and torsional-flexural buckling for members in compression or lateral-torsional buckling for members in bending. In the second step, the reduced member resistance due to global buckling effects is then introduced into the design for global-local buckling interaction (step 2); here, the reduced global buckling resistance is also accounted for by a modified formulation of the relative slenderness for local buckling (see Fig. 3, first column).

Separately, the distortional buckling resistance of the cold-formed cross-section has to be determined in step 3, but without considering interactive distortional-global

buckling. Although the global-distortional interaction of cold-formed cross-sections was clearly observed in tests and numerical simulations [2, 4–8], this effect is ignored in the AISI DSM design approach, this – after consultation with the DSM developers – to avoid too conservative predictions [13]. Finally, the governing design resistance of cold-formed members in compression or bending acc. to AISI DSM results from the minimum value of the pure distortional buckling resistance (step 3) and the interactive global-local buckling resistance (step 2).

3.3 Comparison of the DSM acc. to AISI S100-16, clause E–G, and EN 1993-1-3

Sections 3.1 and 3.2 show that the European and the American design provisions differ fundamentally. This concerns both the general design procedure and the relevant cross-section for the design. A simple comparison of the flow charts in Figs. 2, 3 already shows the significantly greater effort required for the design acc. to EN 1993-1-3.

While an AISI DSM design is always based on the gross cross-section, EN 1993-1-3 requires the determination of an effective cross-section. The effective cross-section represents both the loss of cross-sectional resistance and the changing nonlinear stress distribution observed in experimental, theoretical, and numerical analyses in cross-sections prone to local or distortional buckling. According to EN 1993-1-3, the latter is covered by the shift of the center of gravity from the gross to the effective cross-section. As the AISI DSM design only refers to the gross cross-sections, this phenomenon is not covered in principle. With the revision of the AISI S100-16 in 2016, the design of cold-formed, perforated profiles also became possible (see clause 8). In contrast, the design of perforated members acc. to EN 1993-1-3 has not been sufficiently researched of validated yet.

4 First, simplified draft of a combined DSM/EN 1993-1-3 design approach

4.1 General design procedure

The main objective of the new combined design proposal is to facilitate the design, to completely dispense with the method of effective widths acc. to EN 1993-1-3, and to focus on the gross cross-section when calculating the cross-sectional resistance of cold-formed profiles. Therefore, in a first simple approach, the design provisions of DSM acc. to AISI S100-16 for the consideration of local and distortional buckling are initially introduced without additions into the design provisions acc. to EN 1993-1-3. This simplified approach is shown in Fig. 4.

First, the design resistance $N_{\mathrm{Rk,l}}$ for local buckling is determined acc. to AISI DSM, clause E3.2, based on the gross cross-section (see Eq. (1)). Here, the relative slenderness for local buckling λ_{l} is to be calculated as a function of the plastic axial force N_{pl} of the gross cross-section and the elastic-critical buckling load $N_{\mathrm{cr,l}}$ of the overall cross-section taken from a numerical elastic-critical buckling analysis, e.g., using CUFSM.

$$N_{\mathrm{Rk,l}} = \begin{cases} N_{\mathrm{pl}} & \text{with } \lambda_{\mathrm{l}} = \sqrt{\dfrac{N_{\mathrm{pl}}}{N_{\mathrm{cr,l}}}} \le 0.776 \\ \left[1 - 0.15 \cdot \left(\dfrac{N_{\mathrm{cr,l}}}{N_{\mathrm{pl}}}\right)^{0.4}\right] \cdot \left(\dfrac{N_{\mathrm{cr,l}}}{N_{\mathrm{pl}}}\right)^{0.4} \cdot N_{\mathrm{pl}} & \\ & \text{with } \lambda_{\mathrm{l}} = \sqrt{\dfrac{N_{\mathrm{pl}}}{N_{\mathrm{cr,l}}}} > 0.776 \end{cases} \tag{1}$$

Then, in a similar procedure, the design resistance $N_{\mathrm{Rk,d}}$ is to be predicted acc. to AISI DSM, clause E4, accounting for distortional buckling, Eq. (2).

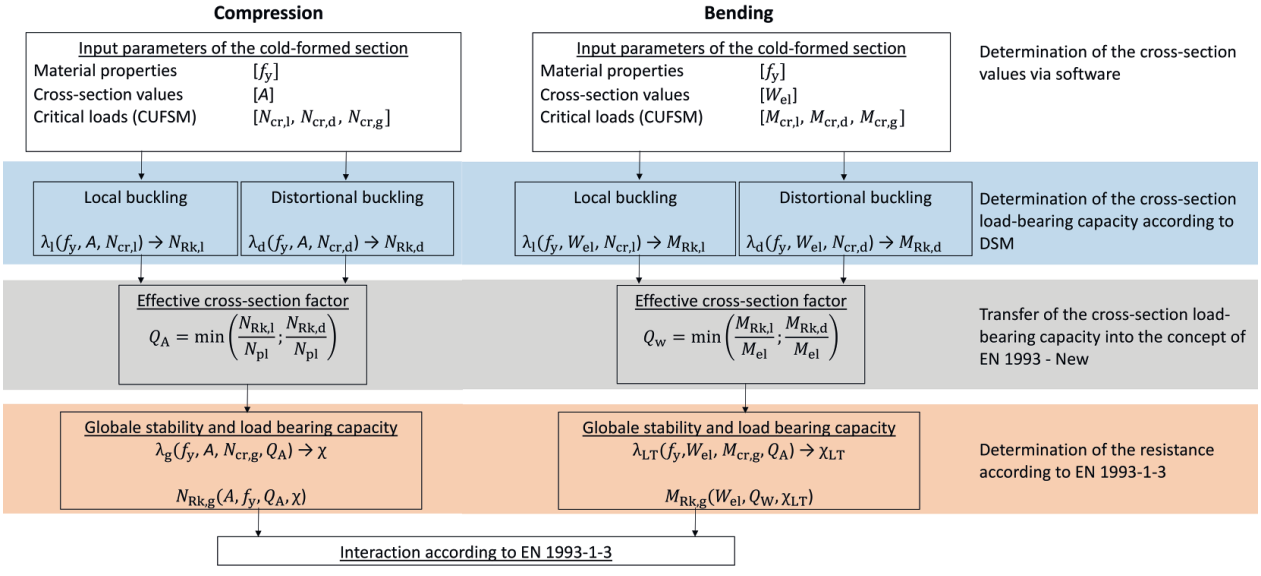

Fig. 4 Flow chart of the design acc. to the simplified, first draft of the combined DSM/EN 1993-1-3 design approach [2]

$$N_{\mathrm{Rk,d}} = \begin{cases} N_{\mathrm{pl}} & \text{with } \lambda_{\mathrm{d}} = \sqrt{\dfrac{N_{\mathrm{pl}}}{N_{\mathrm{cr,d}}}} \le 0.561 \\ \left[1 - 0.25 \cdot \left(\dfrac{N_{\mathrm{cr,d}}}{N_{\mathrm{pl}}}\right)^{0.6}\right] \cdot \left(\dfrac{N_{\mathrm{cr,d}}}{N_{\mathrm{pl}}}\right)^{0.6} \cdot N_{\mathrm{pl}} & \\ & \text{with } \lambda_{\mathrm{d}} = \sqrt{\dfrac{N_{\mathrm{pl}}}{N_{\mathrm{cr,d}}}} > 0.561 \end{cases} \quad (2)$$

However, the next step of the first combined design approach already contains a first adjustment of the AISI DSM design procedure. As an interaction of both local-global and distortional-global buckling interaction of cold-formed sections has been observed in research work [2, 4–8, 14] and should be accounted for in the new approach, the smaller of the previously determined design buckling resistances $N_{\mathrm{cr,l}}$ and $N_{\mathrm{cr,d}}$ for local and distortional buckling was adopted in the subsequent global buckling design. This is in accordance with the principles of EN 1993-1-3, but deviating from AISI DSM, which ignores interactive distortional-global buckling.

An interaction of local and distortional buckling, which is provided for in EN 1993-1-3, is omitted acc. to AISI DSM and the new design approach. Here, the research [2, 4–8, 13] has shown that the interactive local–distortional buckling tends to occur with small, and thus not with practice-relevant component lengths.

To link the design approaches of the AISI DSM and EN 1993-1-3, a so-called Q-factor is introduced, which relates the reduced cross-sectional design resistance for local or distorting buckling of members in compression to the plastic axial force N_{pl} (see Eq. (3)). This Q-factor includes the previously determined cross-sectional resistance of cold-formed sections acc. to AISI DSM and is in principle approximately comparable to the reduced cross-sectional resistance acc. to EN 1993-1-3, which, however, is expressed by the reduced effective area A_{eff} of a section in compression (or effective section modulus W_{eff} for a member in bending).

$$Q_{\mathrm{A}} = \min \begin{cases} Q_{\mathrm{A,l}} = \dfrac{N_{\mathrm{Rk,l}}}{N_{\mathrm{pl}}} \\ Q_{\mathrm{A,d}} = \dfrac{N_{\mathrm{Rk,d}}}{N_{\mathrm{pl}}} \end{cases} \quad (3)$$

The global buckling verification acc. to EN 1993-1-1 [15] can now be conducted, but using the simple reformulations of Eq. (4) for the global slenderness λ_{g} of members in compression. It is shown that the reduced cross-sectional resistance due to local and distortional buckling acc. to EN 1993-1-3, originally expressed via the numerator $A_{\mathrm{eff}} \cdot f_{\mathrm{y}}$, can be replaced by the cross-sectional resistance acc. to AISI DSM, expressed as a function of the Q-factor (see also [16]).

$$\lambda_{\mathrm{g}} = \sqrt{\frac{A_{\mathrm{eff}} \cdot f_y}{N_{\mathrm{cr,g}}}} = \sqrt{\frac{A \cdot f_y}{N_{\mathrm{cr,g}}}} \cdot \sqrt{\frac{A_{\mathrm{eff}}}{A}} = \sqrt{\frac{N_{\mathrm{pl}}}{N_{\mathrm{cr,g}}}} \cdot \sqrt{\frac{A_{\mathrm{eff}} \cdot f_y}{A \cdot f_y}} = \lambda_{\mathrm{g,gr}} \sqrt{\frac{A_{\mathrm{eff}} \cdot f_y}{N_{\mathrm{pl}}}} \sim \lambda_{\mathrm{g,gr}} \cdot \sqrt{Q_{\mathrm{A}}} \quad (4)$$

Based on the global slenderness acc. to Eq. (4), the reduction factor χ for flexural, torsional, or torsional-flexural buckling is to be determined acc. to EN 1993-1-3, clause 6.2, using the European buckling curves for cold-formed sections as defined in EN 1993-1-3, Tab. 6.3.

The final design axial force $N_{\mathrm{b,Rk}}$ of a cold-formed member in uniform compression can be determined acc. to Eq. (5) considering the relevant local-distortional buckling effects on the cross-sectional resistance via the Q-factor (acc. to DSM) and the reduction factor χ for global buckling (acc. to EN 1993-1-3).

$$N_{\mathrm{b,Rk}} = \chi \cdot Q_{\mathrm{A}} \cdot N_{\mathrm{pl}} = \chi \cdot A_{\mathrm{eff}} \cdot f_{\mathrm{yk}} \quad (5)$$

For cold-formed members in bending, the first draft of the combined design approach follows the same principles. After the determination of the cross-sectional resistance, which captures the local and distortional buckling effects based on AISI DSM, a new factor Q_{w}, similar to Eq. (3), is introduced to determine the global slenderness, similar to Eq. (4), and the associated reduction factor χ_{LT} acc. to EN 1993-1-3, which considers the lateral-torsional buckling effects on the member resistance. Finally, the bending moment resistance accounting for coupled instabilities can be calculated using Eq. (6).

$$M_{\mathrm{b,Rk}} = \chi_{\mathrm{LT}} \cdot Q_{\mathrm{w}} \cdot M_{\mathrm{el}} \quad (6)$$

4.2 Summary

In contrast to EN 1993-1-3, which considers an overall interaction of local, distortional, and the governing global buckling, and also in contrast to the DSM, which only covers a local-global buckling interaction, the first draft of the combined design approach considers an interaction of global buckling with the relevant local or distortional buckling mode. In particular, distortional buckling interaction has been shown to be relevant in several researches [2, 4–8]. However, local-distortional interactive buckling is ignored following the DSM provisions and research of Schafer [13].

The combined design approach is based on the gross cross-section throughout; a possible nonlinear stress distribution in the cross-section due to local or distortional buckling is not covered acc. to DSM and is therefore not included in the first draft of the combined design approach. In contrast, effective cross-sections are determined acc. to EN 1993-1-3, which, in principle, considers the modified, nonlinear buckling stresses represented by the shifts in the center of gravity from the gross to the ef-

fective cross-section. This effect has been shown to have a significant influence on the load-bearing capacity of open, simply symmetrical cross-sections [4–6, 17, 18]. It had to be specified and verified in detail as part of the extensive research program in [2].

5 Validation of the first draft for cold-formed members in compression

5.1 Experimental analyses

In the research project [2], a total of 79 column compression test on C- and Ω-shaped cross-sections with or without perforations were conducted, documented in [2: clause 5, Tab. 5-1–5-5, and Annex B]. Compression tests on short- and medium-length columns acc. to EN 1993-1-3, Annex A.3.2 and EN 15512, Annex A.2 [19] are performed to determine the cross-sectional resistance covering local buckling (at short length) and distortional buckling (at medium length). The test lengths were determined acc. to the standard specifications. The member length of short column tests is defined as the triple plate width [1: A.3.2.1. (2)]. For medium-length columns, this included a prior numerical buckling analysis of the cross-section, e.g., using FS software, to determine the test length focusing on approximately pure distortional buckling [1: A.3.2.1. (4)]. Column tests for members with different great lengths used in typical applications are used to investigate the effects of global, interactive local-global or distortional-global effects on the buckling resistance of cold-formed members. All tests serve to observe the phenomenological buckling behavior, to identify the path of buckling modes at different lengths, to capture approximately pure as well as interactive buckling modes, and finally, to determine the load-bearing capacity.

Furthermore, the tests on short- and medium-length tests serve to determine the optimum location of the axial load application by varying the load application on the axis of symmetry until the maximum cross-sectional resistance is achieved. This allows the effect of the nonlinear stress distribution triggered by the local and distortional buckling effects to be captured.

Prior to all compression tests, the test specimens were precisely measured and both the imperfections on the cross-section and over the column length were documented. A summary of the test specimen including all relevant data (section geometry, material, imperfection, etc.) can be taken from [2: clause 5, Tab. 5-2, and Annex B].

In addition, in preliminary studies tensile tests acc. to EN ISO 6892-1 [20] were conducted on comparable cold-formed cross-sections. The tests were conducted on test specimens taken from both the coil before cold forming and from sections from the cold-formed areas, to analyze the influence of strain hardening. Stress-strain diagrams were prepared, via which the relevant material parameters yield strength f_y, tensile strength f_u, and Young's modulus E were determined [2: clause 4 and Annex A].

The test setup used for compression tests is exemplarily illustrated in Fig. 5 for medium-length column test on an Ω-shaped rack upright. The uprights were welded to thick-walled base and cap plates on both sides at their end. Axial spherical plain bearings serve to realize a simple support. The load was applied via the welded cap plates, which were bolted to a connecting plate using slotted holes to shift the location of the applied axial load (see Fig. 5a).

As an example, but representative of most compression tests conducted in [2], Fig. 6 shows the failure patterns of a C-shaped cross-section A_288_30 of thickness $t = 3$ mm (material: S390GD+Z, $f_{y,test}$=396 N/mm^2) in compression tests with different lengths (columns lengths between end plates 320/850/1550/1850 mm; corresponding system length between axial spherical plain bearings: 365/895/1595/1895 mm) after testing and unloading. As expected, pure local buckling was the predominant buckling mode for short columns. At medium length, distortional buckling dominated. Members at long length were prone to flexural-torsional buckling dominates or interac-

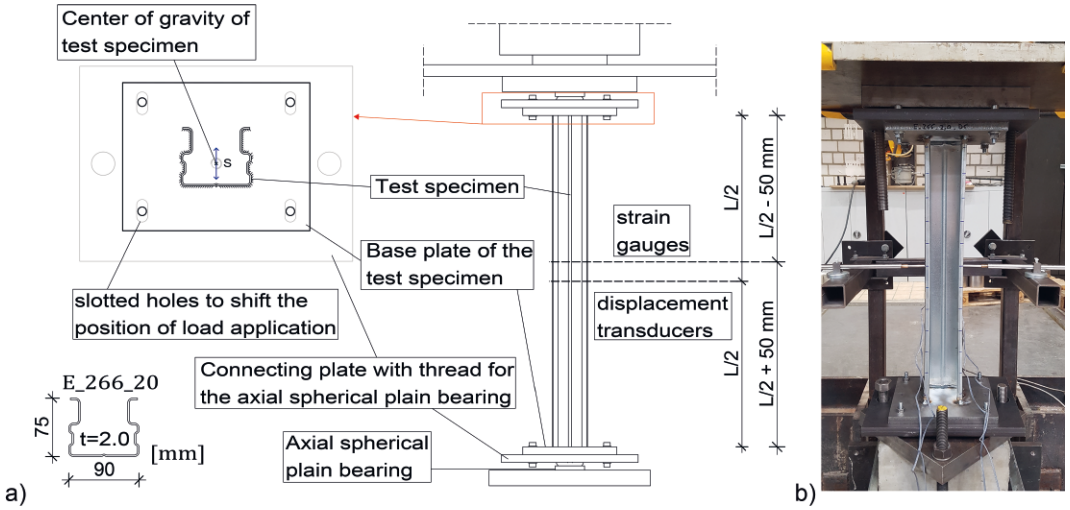

Fig. 5 Test setup of the compression tests: a) construction sketch with realization of the load application; b) Ω-shaped cross-section E_288_20 in the test setup

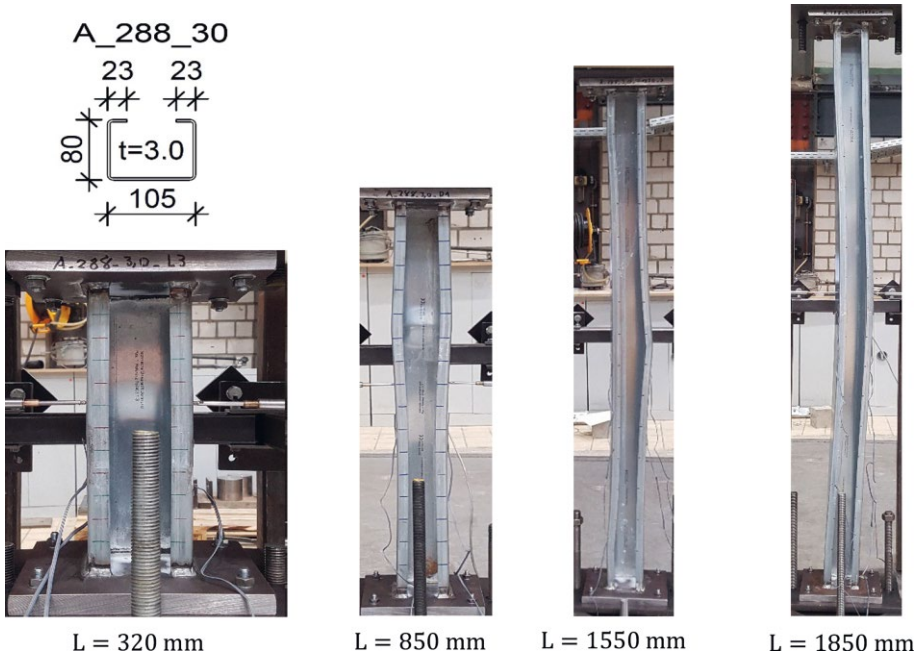

Fig. 6 C-shaped cross-section A_288_30 in all examined lengths after unloading (see [2: clause 5, Fig. 5–15])

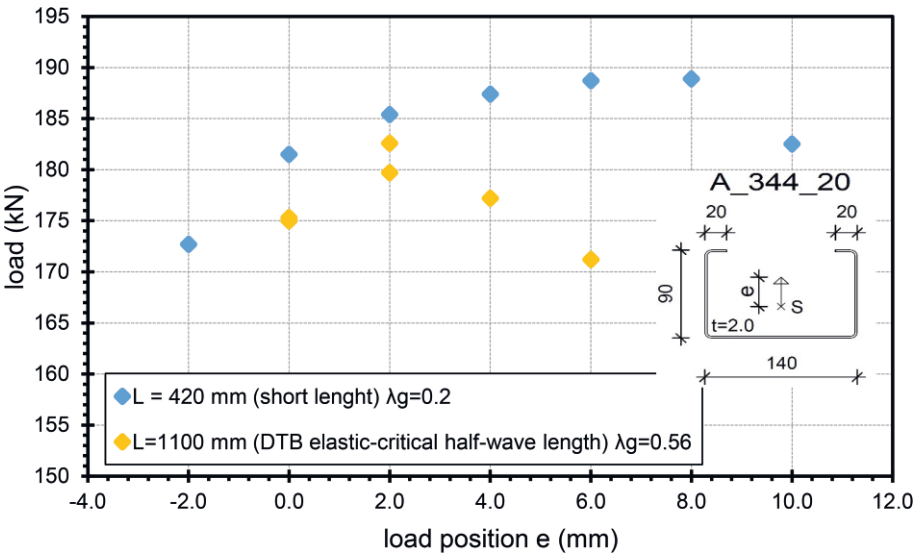

Fig. 7 Load capacity depending on load application point for A_344_20 in the length $L = 420$ mm and $L = 1100$ mm

tive distortional-global buckling, the latter more especially for medium (L = 1550 mm) than for long column lengths (L = 1850 mm). The tests conducted in [2] proved that for common member lengths of cold-formed cross-sections, an interaction of distortional buckling and flexural-torsional buckling occurs and should therefore not be ignored in a design procedure (see [2: clause 5, Tab. 5-3–5-5]).

The compression tests on stub and medium-lengths columns, conducted acc. to the test specifications in EN 15512, Annex A2.1/A2.2, with variation of the load application point of the axial force on the symmetry axis, confirmed the shift of the internal compressive force resultants in cross-sections prone to local and distortional buckling. As an example, Fig. 7 shows the cross-sectional resistance of a C-shaped section A_344_20 with thickness $t = 2$ mm and a small specimen lengths of 420 mm (material: S390GD+Z, $f_{y,test}$=396 N/mm^2), where local buckling dominated in the test and the maximum cross-sectional resistance was reached when the axial load was applied at a distance of 8 mm from the center of gravity of the gross cross-section. With an increasing, medium member length of 1100 mm and dominating distortional buckling effects, the maximum cross-sectional capacity was achieved at a distance of only 2 mm. The effect of the shift of the internal compressive force resultants in cross-sections prone to local and distortional buckling was found to be essential.

5.2 Validation of the first, simplified draft of the combined design approach based on tests

The first, simplified draft of the combined design approach acc. to clause 4 was validated based on the exten-

sive results of the test series [2: clause 5.2, Tab. 5-6, 5-7]. It was compared to the design predictions acc. to EN 1993-1-3 and AISI DSM as well. As an example, significant test results compared to different design approaches for selected C- and Ω-shaped cold-formed sections at different member lengths are summarized in Fig. 8. To record the special boundary conditions in the tests accurately and to obtain realistic design results, at this point the FE software ANSYS (2020 R2) [21] was used to calculate the elastic-critical buckling loads, which were equally introduced into the respective design approaches. In later comparative calculations, the FS software CUFSM (5.04) [12] was used (see [2: p. 100–103]).

For better comparability of the different design provisions, partial safety factors were ignored and a uniform Young's modulus of 210.000 N/mm^2 was applied. As global imperfections of the tested members measured before testing were quite low (see [2: clause 5, Tab. 5-2]), European buckling curve *a* was assumed for a comparative global buckling prediction acc. to both EN 1993-1-3 and the first draft of the combined design approach. This assumption was also confirmed by comparing the test results of the long members, where almost pure global flexural torsional buckling was observed in tests, with the buckling design acc. to EN 1993-1-3 based on the European buckling curves (EBC) in [2: clause 5.2, Fig. 5-35]. However, the adjustment of the EBC classification was used exclusively to recalculate the test results (to consider component tests under ideal laboratory conditions). A general change of the classification of cold-formed steel sections in the EBC is not intended.

Fig. 8 shows that the predictions for short columns in compression acc. to both AISI DSM and the first draft of the new combined design approach can overestimate the cross-sectional resistance from tests, i.e., when local (-distortional) buckling is the governing buckling mode. In-depth analyses in [2: clause 5.2, e.g., Fig. 5-36] revealed that the simplified DSM design approach, which neglects the shift of the compressive force resultants, typical of small- and medium-length symmetrical sections prone to local and distortional buckling, is the main cause for the nonconservative design predictions. It became clear that this first simplified draft of the combined design approach, based on the local and distortional buckling design acc. to AISI DSM, is not satisfactory and needs to be revised. This conclusion confirms the assumptions after the initial investigations of ECCS TWG7.5 [4–8]. However, with increasing member length and dominant global buckling, both design approaches become significantly more conservative compared to the test results; here, the influences from the relevant distortional or, in particular, local buckling modes and thus the non-unfavorable effect of the nonlinear stress distributions across the cross-section are significantly lower.

In contrast, the design provisions of EN 1993-1-3, which cover all possible local-distortional-global buckling effects and use the rather conservative European buckling curves for the global buckling design, give the lowest load-bearing capacities for all tested cross-sections, irrespective of the member length, and appear clearly too conservative compared to the tests, despite the high design effort.

In addition, the column tests showed that interactive global-distortional buckling occurs in almost all medium and large length C- and Ω-shaped profiles investigated (see [2: clause 5, Tab. 5-3–5-5]). This significant effect is ignored in the pure AISI DSM design, but has already been included in the first simplified combined design approach acc. to clause 4, Fig. 4, based on research [4–8]. As a comparison of the AISI-DSM results with the predictions acc. to the initial combined design approach from clause 4 shows, higher load capacities are often predicted acc. to AISI DSM (however, this general statement has to be specified in detail for individual cases, considering the different normative global buckling curves).

For further information and all relevant data on the design predictions compared to the tests conducted for validation, reference is made here to [2: clause 5.2, Tab. 5-6, 5-7]. The results presented in the clauses 5.1/5.2 of this article only serve as an exemplary, but representative presentation and confirmation of the procedure.

5.3 FE model and numerical analyses

Numerical models were developed using the FE software ANSYS (2020 R2) [21] for in-depth analysis of the load-bearing capacity and buckling behavior of the tested column sections. For an accurate calibration of the numerical model based on the test results, cross-sectional and global member imperfections as well as material properties of the specimens measured before the tests were implemented in the FE model (see [2: clause 8, Fig. 8-3–8-5]). The effect of strain hardening in the cold-formed areas of

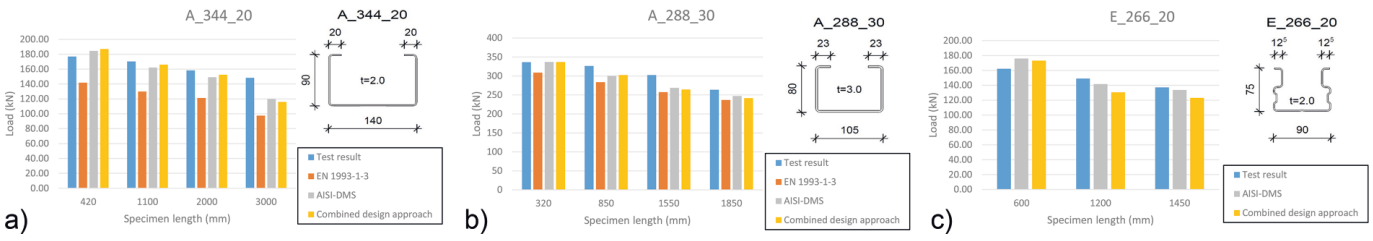

Fig. 8 Comparison of the design acc. to EN 1993-1-3, AISI DSM and the combined approach with the test results for test specimen: a) A_344_20 (S390GD+Z); b) A_288_30 (S390GD+Z); c) E_266_20 (S350GD+Z) [2: Fig. 5–31]

the profiles [22–30], which was investigated by tensile tests (see [2: clause 4 and Annex A]), is considered by dividing the cross-sections into strain-hardened and plane, unworked areas. In the plane areas, the measured material parameters were applied and in the corner areas, the material parameters were calculated acc. to EN 1993-1-3, 3.2.2. In [2: clause 4, Fig. 4-9], it was shown that this formula could capture the hardening in a good approximation. As a representative example, Fig. 9 shows the numerical FE model of an Ω-shaped cross-section including the detailed implemented material specifications and reflecting the support conditions in the tests. The test specimens, including base and cap plates, were modelled with ANSYS shell elements no. 181. As in the column compression tests, the axial load was applied via the thick-walled end plates. The member was vertically and laterally supported in the center of the column base. The symmetry axis of the cap plates was fixed in the *z*-direction; a displacement in the *y*-direction was blocked at the location of the load application. This modelling generates simple support conditions. For a more detailed description of the numerical model, the reader is referred to [2: clause 8, p. 163–169].

Numerical simulations and parameter studies had been conducted to calibrate the numerical models. Furthermore, in-depth analyses of the load-bearing and buckling behavior of cold-formed sections were conducted and compared to the test results. It can be summarized that the FE simulations conducted generally showed very good agreement with the results observed in tests in terms of load-bearing capacity, deformations, and phenomenological buckling behavior. This statement is confirmed exemplarily by Fig. 10 in which the measured deformations of an Ω-shaped cross-section E_266_20_P (material: S350GD+Z) in compression acc. to tests are illustrated and compared to FE simulations. In the course of the research project [2], numerical simulations were conducted for all cold-formed sections and columns that were investigated experimentally (see [2: clause 8, Tab. 8-2, 8-3]). In this way, the validation of the developed FE model could be comprehensively confirmed.

5.4 Numerical parameter studies for general validation and optimization of the combined design approach

Based on the calibrated FE model, numerical parameter studies were conducted which served for a targeted validation and optimization of the combined design approach for cold-formed C- and Ω-shaped sections. If the FE analyses focused on the tested sections, e.g., considering additional member lengths, the initial calibrated numerical models was used including geometric imperfections and material properties as measured to obtain realistic predictions compared to tests. For general parametric studies with focus on cold-formed cross-sections in various dimensions, material, and member lengths, which

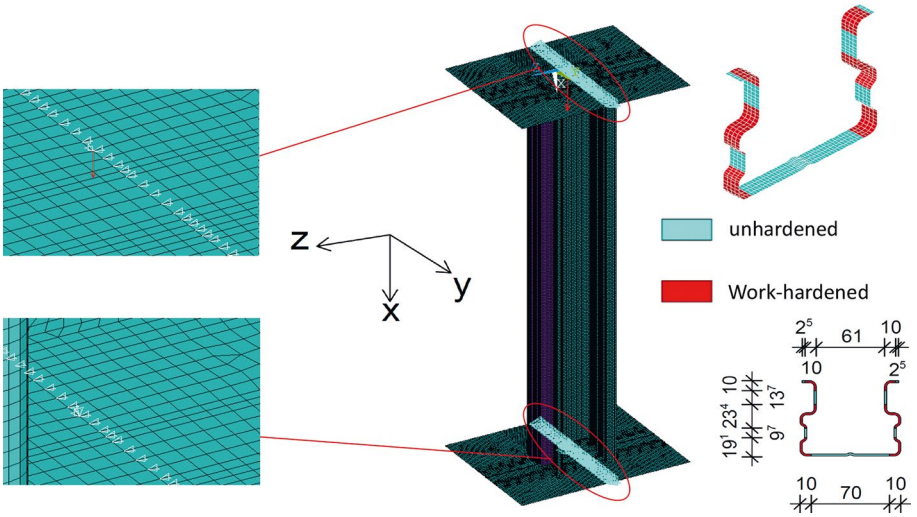

Fig. 9 Numerical model for an Ω-shaped cold-formed cross-section including an approach of material hardening (ANSYS 2020 R2)

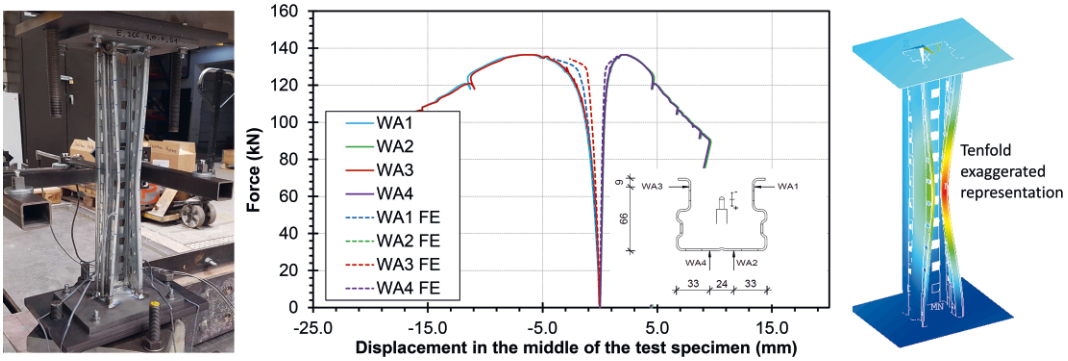

Fig. 10 Results of tests and simulations for an Ω-shaped cross-section E_266_20_P in compression (see [2: clause 8, Fig. 8-6])

were not tested in [2], the calibrated numerical model was also used, but nominal material parameters and Young's modulus of E = 200.000 N/mm^2 were applied. Strain hardening in the cold-formed corner areas was considered, using the simplified average yield strength acc. to EN 1993-1-3 in the area of the rounded corner. In addition, equivalent geometric imperfections were implemented in accordance with the EN 1993-1-5, with reference to the National Annex of EN 1993-1-1 [31], i.e., buckling shapes according to a previous elastic-critical buckling analysis with w_0=a/200 for local buckling of plane elements and a sinusoidal shape with L/350 for global buckling. As EN 1993-1-5 does not contain an imperfection approach for distortional buckling, Walker's equations [32, 33] for distortional buckling were used. According to EN 1993-1-5, the imperfections of the different modes were superimposed in such a way that only the governing imperfection was set at 100 % and the others at 70 % (see [2: clause 8.3, p. 186–188]). According to prEN 1993-1-14 [34], residual stresses were not applied for cold-formed sections. Detailed information on the general modelling can be taken from [2: clause 8].

In a first parametric study on thin-walled, simply symmetrical, open cross-sections with small and medium lengths in compression, the effect of the changing, nonlinear compressive stresses due to local and distortional buckling was analyzed as a result of the findings described in clause 3.1 and 5.2 (see [2: clause 8.3, p. 182–185]). Both tests acc. to clause 5.1 and FE parametric simulations generally prove that the maximum cross-sectional resistance is typically achieved when the axial load is applied eccentrically to center of gravity of the gross cross-section. It is also shown that the optimum location of the load application changes with different member lengths [2: clause 8.3, Fig. 8-20, 8-22]. Fig. 11 (left) shows the optimum load position of the tested Ω-shaped section E_266_20 (material: S350GD+Z) in axial compression with lengths of 400 to 1600 mm, related to the center of gravity of the gross cross-section, at which the largest cross-sectional resistance was achieved in the FE simulations. The largest eccentricity of the internal axial force was numerically recorded at a member length of 600 mm. This value corresponds to the half-wavelength for elastic distortional buckling which is the relevant buckling mode acc. to FS analyses in this case. However, local-distortional buckling effects decrease with increasing member lengths where global buckling effects become dominant. FE simulations ([2: clause 8, p. 182–185]) and Fig. 11 (left) confirm that the maximum buckling resistance is then obtained when the axial load is applied approximately at the center of gravity of the gross cross-section. This conclusion is consistent with the outcomes of the tests (see Fig. 8).

Fig. 11 (right) shows the results of a comprehensive, general FE parametric study for C- and Ω-shaped sections in compression compared to the design predictions acc. to the first draft of the combined design approach acc. to clause 4. The design buckling resistances compared with the ultimate capacities acc. to FE simulations are recorded as a function of the factor Q_A/χ. According to clause 4, Eq. (3), Q_A has been defined as the reduction factor for the cross-sectional resistance accounting for local-distortional buckling. χ is known as the reduction factor for global buckling acc. to EN 1993-1-3. Fig. 11 (right) shows that a lot of nonconservative predictions acc. to the combined design approach occur for ratios $Q_A/\chi \leq 1.0$, i.e., for thin-walled cold-formed sections where local-distortional buckling dominates. On the other hand, the new combined design provision was confirmed when global buckling dominates and the shift of the center of gravity due to nonlinear stresses is negligibly small.

In summary, with the help of the parametric FE simulations for a wide variety of cold-formed steel cross-sections, the initial theoretical analyses (Sections 1 and 4) and from the experimental investigations (Section 5.2) could be generally confirmed now. However, to exclude any nonconservative design predictions, the simplified combined design approach was further improved based on the scientific findings on the decisive cause, which was found to be the neglect of the nonlinear stress effect in cross-sections prone to local-distortional buckling.

6 Experimental and numerical analyses for cold-formed members in bending

In the course of the research project P1328/IGF 19964 [2], four-point bending tests on C-, Z-, and Ω-shaped cold-formed sections with and without perforations are con-

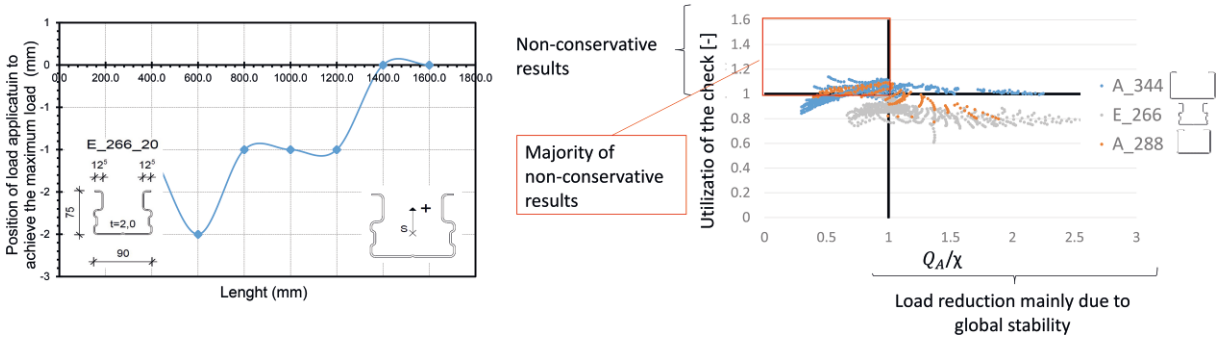

Fig. 11 Left: Results of the numerical simulations for an Ω-shaped section E_266_20 (material: S350GD+Z) in compression [2: clause 8, Fig. 8–20]; right: comparison of numerical simulations with the predictions acc. to the first draft of the new combined design approach for C- and Ω-shaped cross-sections as a function of value Q_A/χ see clause 4 [2: clause 8, Fig. 8–35])

ducted acc. to EN 1993-1-3, Annex A, and EN 15512, A.2.5, to also investigate the design buckling resistance in major-axis bending. As all tested sections are monosymmetrical or asymmetrical sections, a "doubled" test setup was realized in accordance with EN 15512, A.2.9, which allows the application of a vertical load approximately without torsional loading for the tested beams (Fig. 12).

The tests were conducted at different lengths and the ultimate loads obtained were compared with predictions acc. to EN 1993-1-3, DSM and the draft of the new combined design approach from clause 4.1. As an example, the results are shown in Fig. 13 for two different C-sections A_288 with thickness 3.0 mm and A_344 with thickness 2.0 mm (each material: S390GD+Z). In addition, a numerical model using ANSYS (2020 R2) acc. to clause 5.3 was developed, calibrated on the bending tests, and used for further numerical parameter studies, which confirm the fundamental outcomes of the experimental investigations.

Fig. 13 is intended here only as an exemplary, but representative example of the analyses in [2]. In summary, it can be stated that the general conclusions of the investigations on cold-formed components in compression and bending are very similar: both the DSM and the combined design approach give nonconservative results for cold-formed sections at short and medium length when local or distortional buckling becomes dominant. For further data and analyses on scientific investigations on members in bending, see [2: clause 6]. More result (comparison of the design approaches with tests) can be found in [2: clause 6.2, Fig. 6-35–6-37, Tab. 6-5]. An adaptation of the first draft of the combined design approach for cold-formed section in bending (clause 4) was also required.

7 Final improvement of the combined AISI DSM/ EN 1993-1-3 design approach

7.1 Derivation of an improved, final combined design approach

According to the outcomes of the experimental and numerical investigation described in clause 5, the lack of consideration of the nonlinear stress distribution due to local and distortional instabilities has turned out to be the crucial source of error for the first draft of the combined design approach, especially for cold-formed sections at small and medium member length. This effect decreases significantly with increasing member length and becomes nearly negligible for long members. To account for this effect, the first draft of the new combined design approach was extended by reduction factors χ_{eN} for members in axial compression and χ_{eM} for members in bending (see Eq. (7), (8)). These newly introduced factors reduce the design buckling resistance acc. to the scientific investigations in [2] whenever local and distortional buckling of cold-formed cross-sections (represented by the Q-factor acc. to Eq. (2)) become dominant compared with global buckling effects (represented by χ and χ_{LT} acc. to EN 1993-1-3).

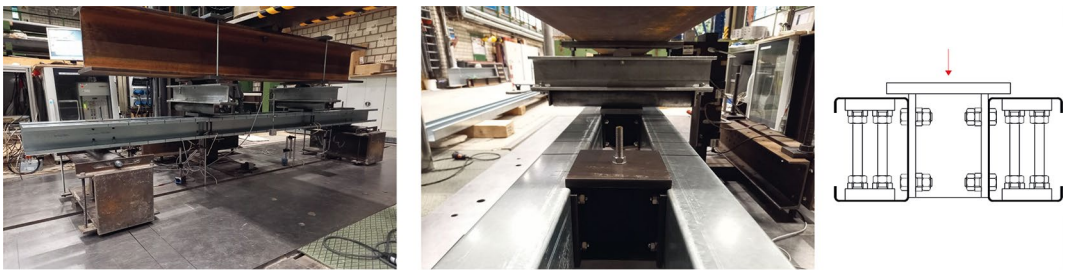

Fig. 12 Test setup of the four-point bending tests acc. to EN 15512 and detail of the load application for C-shaped sections

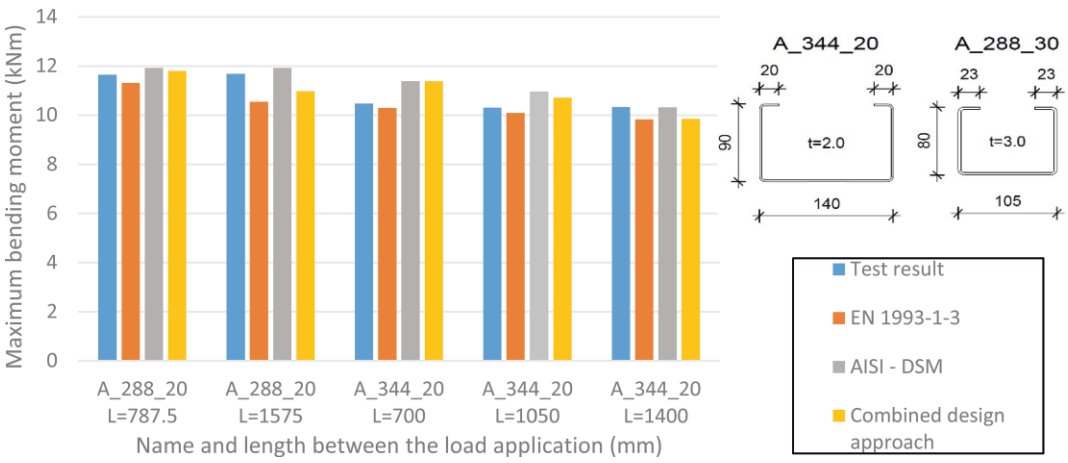

Fig. 13 Comparison of the design acc. to the combined design approach, EN 1993-1-3 and AISI DSM with the test results for C-shaped cold-formed cross-sections in bending (see [2: Fig. 6-35])

$$\chi_{eN} = \max\left[1 - \chi + Q_A; 0.85\right] \leq 1.0 \quad (7)$$

$$\chi_{eM} = 1 - \chi_{LT} + Q_w \leq 1.0 \quad (8)$$

This results in the new Eq. (9) and (10) for predicting the design resistances for cold-formed members in compression and bending prone to coupled local-distortional-global instabilities as follows:

$$N_{b,Rk} = \chi \cdot Q_A \cdot N_{pl} \cdot \chi_{eN} \quad (9)$$

$$M_{b,Rk} = \chi_{LT} \cdot Q_w \cdot M_{el} \cdot \chi_{eM} \quad (10)$$

7.2 Final validation of the improved combined design approach

The improved final combined AISI DSM/EN 1993-1-3 design approach acc. to clause 7.1 was finally validated for all previously investigated cold-formed cross-sections and members based on both the test results of clause 5.1/6 and the numerical simulations (see Clause 5.2/6).

As a representative example for the evaluation, Fig. 14a–c shows a comparison of the predictions acc. to the first draft of the combined design approach (clause 4) with the final improved combined design approach (clause 7.1) for C- and Ω-shaped cross-sections in compression, additionally contrasted with test results from [2: clause 9.3]. As it will be common in the practical application later, the elastic-critical buckling loads are calculated with CUFSM (Version 5.04) instead of ANSYS (for further information of the assumptions made, see [2: clause 5, p. 100-102]). Fig. 14 illustrates that the design buckling resistances of compressed members in coupled instabilities can be slightly reduced by the new factor χ_{eN} in a targeted manner; nonconservative predictions for small- and medium-length columns can now be avoided. Especially the exam-

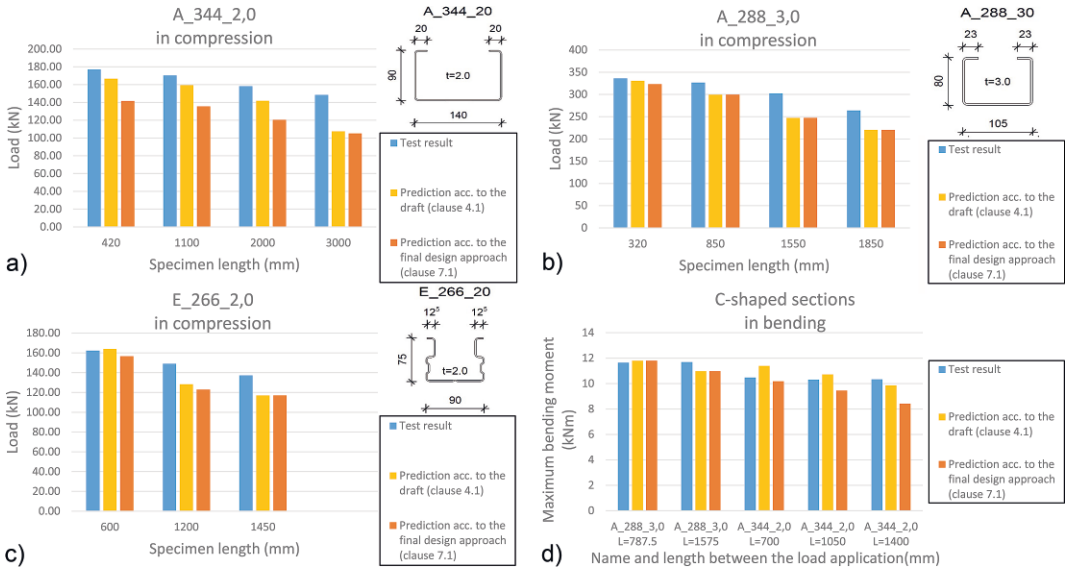

Fig. 14 Comparison of the predictions acc. to the combined design approach and acc. to the draft to the test ultimate load: a) A_344_20 (material: S390GD+Z) in compression; b) A_288_30 (material: S390GD+Z) in compression; c) E_266_20 (material: S350GD+Z) in compression; d) C-sections (material: S390GD+Z) in bending (see [2: clause 9])

Compression								Pictograms of the cross sections
Section	Material	Length [mm]	statisitical evaluation of the normalized test results N [kN]	combined design approach				
				λ_l	λ_d	λ_g	Load capacity N [kN]	
A_288_30	S390GD+Z	320	336.22	0.54	0.64	0.18	323.27	
		850	326.50	0.54	0.71	0.44	299.87	
		1550	302.49	0.54	0.76	0.78	247.42	
		1850	263.86	0.54	0.76	0.92	220.46	
A_344_20	S390GD+Z	420	176.98	1.11	1.24	0.15	141.63	
		1100	170.30	1.11	1.24	0.39	135.49	
		2000	158.21	1.11	1.24	0.69	120.44	
		3000	148.39	1.11	1.24	1.03	105.04	
E_266_20	S350GD+Z	600	162.27	0.28	0.75	0.38	156.63	
		1200	149.03	0.28	0.91	0.7	122.93	
		1450	137.25	0.28	0.91	0.84	116.95	
E_266_20_P	S350GD+Z	600	126.84	0.35	0.81	0.41	131.12	
		1100	123.46	0.35	1.00	0.73	113.43	
		1300	114.04	0.35	1.00	0.85	103.66	
Bending								
Section	Material	Length between load application [mm]	statisitical evaluation of the normalized test results M [kNm]	combined design approach				
				λ_l	λ_d	λ_{LT}	Load capacity M [kNm]	
A_288_30	S390GD+Z	687.5	11.65	0.39	0.58	0.51	11.73	
		1475	11.69	0.39	0.49	0.24	10.48	
A_344_20	S390GD+Z	600	10.47	0.67	0.82	0.19	10.17	
		950	10.30	0.67	0.87	0.30	9.47	
		1300	10.33	0.67	0.95	0.39	8.44	

Fig. 15 Extract from the results of compression and bending tests of cold-formed sections from [2: clause 9, Tab. 6-5], compared to the predictions acc. to the improved final combined AISI DSM/EN 1993-1-3 design approach (see clause 7.1)

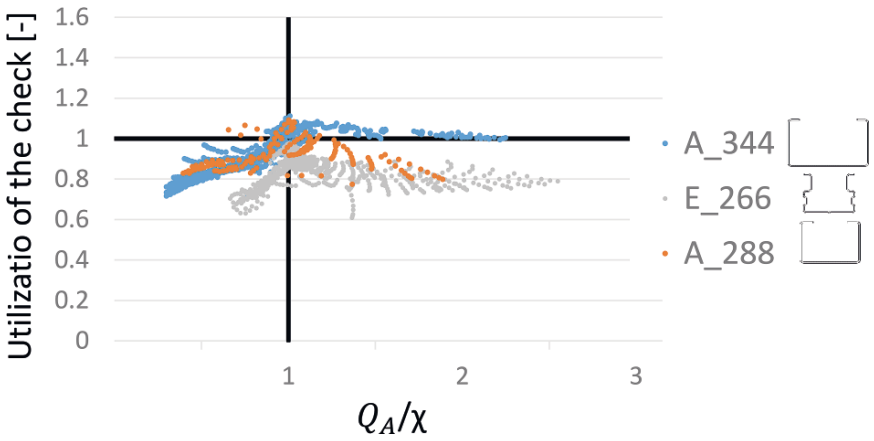

Fig. 16 Comparison of the predictions acc. to the final improved combined design approach to the results of numerical parameter study for C- and Ω-shaped sections in compression (see [3: clause 9.3.2])

ple Fig. 14d of the C-shaped section A_344_20 in bending shows the importance of the new reduction factor χ_{eM}. Due to the thin-walled nature of this cross-section and the thus prevailing local-distortional buckling effects, the application of χ_{eM} introduced to account for the nonlinear buckling stresses observed in tests, and the corresponding reduction of the design buckling resistance is essential to obtain reliable predictions acc. to the final improved combined design approach. By definition and in agreement with the investigations of clause 5 to 6, the design of long members susceptible to dominant global buckling is not affected by this amendment.

Fig. 15 gives important information on the specimen and tests presented in this article which are used for validation. In addition, the test results are presented compared to the predictions acc. to the final improved combined AISI DSM/EN 1993-1-3 design approach of clause 7.1. Further test data (material, imperfections, etc.) can be found in [2: clause 9, Tab. 9-2, and Annex B, C].

Finally, as already demonstrated in Section 5.4, the predictions acc. to the improved final combined design approach were again generally compared with the results of the basic, extensive FE-based parametric studies applied for determining the load-bearing capacity and buckling behavior of a wide variety of cold-formed steel cross-sections and member lengths. The evaluation, exemplified by Fig. 16 for C- and Ω-shaped cross-sections subjected to axial compression, now also proves in general that with the improved final combined design approach and by introducing the new factor χ_{eN}, a nonconservative design can be avoided. Nevertheless, some slightly nonconservative predictions in the range of $Q_A/\chi \approx 1.0$ were still obtained.

However, as the simulations were generally rather conservative compared to the test results, the improved final combined design approach is evaluated as convincing and acceptable. For in-depth evaluation of tests, test data, and numerical parameter studies for cold-formed sections in bending, see [2: clause 6, 8.2.2, 8.3, 9].

8 Applicability of the combined design approach to members with perforations

The final improved combined AISI DSM/EN 1993-1-3 design approach is also applicable for the design of perforated sections, as new design provisions for DSM were introduced with AISI S100-16 in 2016. On the one hand, the DSM generally allows for determining the elastic-critical buckling loads for cross-sections with perforations. In addition, the AISI DSM approach, clause E3.2.2, E4.2, F3.2.2, and F4.2, can be used to predict the final cross-

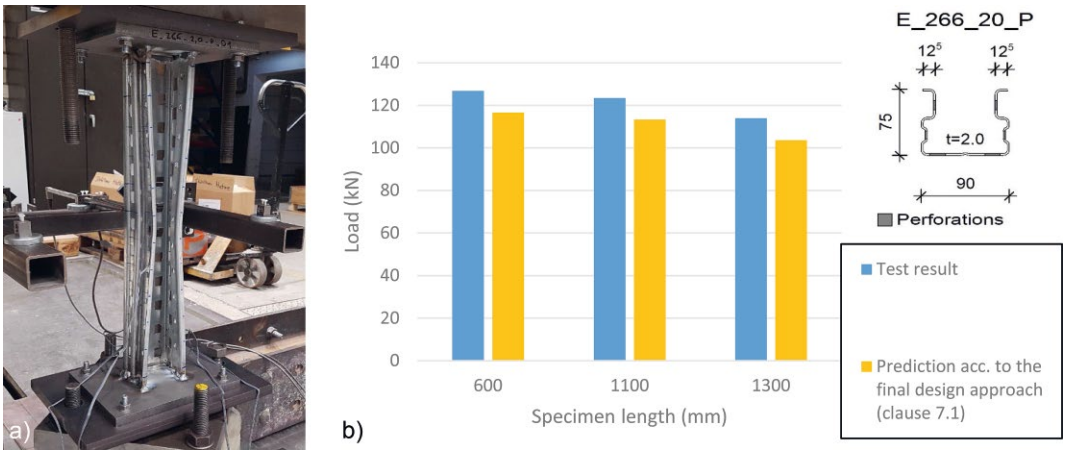

Fig. 17 Perforated cold-formed profiles: a) Ω-shaped test specimen; b) comparison of the predictions acc. to the combined design approach to the test results

sectional resistance of perforated cross-sections prone to local and distortional buckling.

For the calculation in [2], the Finite-Strip-Software CUFSM (5.04) [12] should be used. However, as the influence of the perforations on the elastic-critical buckling loads cannot be neglected [35], the proposal of Casafont et al. [36] is taken up in [2]. This proposal proved that the perforated areas are simplified modelled by equivalent thicknesses so that conventional FSM can be used to estimate and analyze the buckling behavior of cross-sections with perforations. The program CUFSM is under continuous development, with research being done on the implementation of perforation [37].

The improved final combined design approach of clause 7.1 was adapted acc. to the new provisions of AISI S100-16 and accordingly extended for perforated cross-sections [2: clause 9.2]. Fig. 17 shows an example of the test results of a perforated Ω-shaped section E_266_20_P in compression at different lengths compared to the predictions acc. to the new design approach. Satisfactory predictions can be achieved here as well, so that this simple extension of the design approach can be recommended for practical application. For further tests and test data on perforated profiles (including measured imperfections, material properties) as well as corresponding predictions acc. to the extended final combined design approach, see [2: clause 5, Tab. 5-2, 5-4, 5-5, clause 9, p. 219–227].

9 Summary and conclusion

A design approach for cold-formed steel sections in coupled instabilities is presented, which was developed in the course of the research project FOSTA P1328/IGF 19964. It combines the advantages of the Direct Strength Method, taken from AISI S100-16, with the design provisions of EN 1993-1-3. With the help of AISI DSM, which usually uses elastic buckling analyses based on finite strip methods, the cross-sectional resistance of cold-formed profiles prone to local and distortional buckling is predicted. The complicated, time-consuming determination of effective cross-sections acc. to EN 1993-1-3 is omitted. The global buckling design considering flexural, torsional, torsional-flexural or lateral-torsional buckling is conducted acc. to the European standard EN 1993-1-3, so that the new combined design approach can easily be introduced into EN 1993-1-3.

New adjustment factors Q were introduced to implement the cross-sectional resistances calculated acc. to DSM in the European standard (see Eq. (3)). Additional reduction factors χ_{eN} and χ_{eM} serve to cover the effects of the nonlinear local and distortional buckling stresses in thin-walled cross-sections prone to local and distortional buckling (see Eq. (7), (8)).

Within the framework of [2], experimental investigations and numerical FE analyses were conducted for cold-formed sections with and without perforations at different lengths to analyze the buckling phenomena and determine the load-bearing capacity of thin-walled profiles in pure or interactive buckling. For validation, the buckling resistances obtained from tests and FE studies were compared with the predictions of the final combined design approach, which has thus been shown to provide reliable buckling resistances of cold-formed sections prone to buckling instabilities.

With a view to the daily design in engineering practice, the new combined design approach is evaluated as simple, user-friendly, less error-prone, time-saving, and efficient. A normative implementation into the existing European standard EN 1993-1-3 is easily possible.

Acknowledgements

The research project IGF no. 19964 N/FOSTA P1328 "Future viability of cold-formed steel sections in building structures" of the Research Association for Steel Application (FOSTA), Sohnstraße 65 in 40237 Düsseldorf, Germany, was funded by the German Federation of Industrial Research Associations (AiF) as part of the program for the promotion of Industrial Collective Research (IGF) by the Federal Ministry of Economic Affairs and Climate Action on the basis of a decision by the German Bundestag.

Open access funding enabled and organized by Project DEAL.

References

[1] EN 1993-1-3 (2010) *Eurocode 3: Bemessung und Konstruktion von Stahlbauten – Teil 1-3: Allgemeine Regeln – Ergänzende Regeln für kaltgeformte Bauteile und Bleche.* Berlin: DIN Deutsches Institut für Normung e.V.

[2] Ungermann, D.; Lemański, T.; Brune, B. (2022) *Zukunftsfähigkeit von kaltgeformten Stahlprofilen im Bauwesen.* IGF-Nr. 19964 N, FOSTA P1328.

[3] AISI S100-16 (2016) *North American Specification for the Design of Cold-Formed Steel Structural Members.*

[4] ECCS TC 7 – TWG 7.5-2015-008; Brune, B. (2015) *Design of cold-formed steel members: DSM combined with EN 1993-1-3.*

[5] ECCS TC 7 – TWG 7.5-2015-009; Dubina, D.; Ungureanu, V. (2015) *Application of DSM into EN 1993-1-3 format for stability checking of cold-formed Members: Compression, Bending and Bending Compression*.

[6] ECCS TC 7 – TWG 7.5-2015-010; Casafont, M. et al. (2015) *DSM and its adaption to Eurocode 3-1-3.*

[7] ECCS TC 7 – TWG 7.5-2016-004; Casafont, M. (2016) *European and American Design Procedure for Pallet Rack Upright Frames.*

[8] ECCS TC 7 – TWG 7.5-2016-005; Brune, B. (2016) *Combined DSM-EC3 approach for the design of cold-formed sections and members.*

[9] ECCS TC 7 – TWG 7.5-2022-008; Brune, B.; Lemański, T. (2022) *Simplified DSM/EC3 approach for rack uprights compared to tests.*
[10] Ungermann, D.; Lemański, T.; Brune, B. (2022) *A new Eurocode-compliant Design Approach for Cold-Formed Steel* Sections. The International Colloquium on Stability and Ductility of Steel Structures. ce/papers 5, No. 4, pp. 125–134.
[11] EN 1993-1-5 (2019) *Eurocode 3: Bemessung und Konstruktion von Stahlbauten – Teil 1-5: Plattenförmige Bauteile.* Berlin: DIN Deutsches Institut für Normung e.V.
[12] CUFSM (2020) *Cross-Section Elastic Buckling Analysis, Version 5.04 [software].* Thin-walled Structure Group, Civil and Systems Engineering, Johns Hopkins University. https://www.ce.jhu.edu/cufsm/downloads/
[13] Schafer, B.W. (2008) *Review: The direct strength method of cold-formed steel member design.* Journal of Constructional Steel Research 64, No. 7, pp. 766–778.
[14] Young, B.; Rasmussen, K. (1998) *Test of cold-formed channel columns.* Fourteenth International Specialty Conference on Cold-Formed Steel Structures.
[15] EN 1993-1-1 (2010) *Eurocode 3: Bemessung und Konstruktion von Stahlbauten – Teil 1-1: Allgemeine Bemessungsregeln und Regeln für den Hochbau.* Berlin: DIN Deutsches Institut für Normung e.V.
[16] Brune, B.; Clasen, S. (2018) *Die Einführung der Direct Strength Method zur Bemessung von kaltgeformten Stahlprofilen nach EN 1993-1-3.* Stahlbau 87, No. 4, pp. 297–307. https://doi.org/10.1002/stab.201810585
[17] Brune, B.; Peköz, T. (2013) *Design of cold-formed steel members – Comparison of EN 1993-1-3 and direct strength method.* Steel Construction 6, No. 2, pp. 82–94. https://doi.org/10.1002/stco.201310020
[18] Young, B. (2004) *Local buckling and shift of effective centroid of slender sections.* Proceedings of the 1st International Symposium on Worldwide Codified Design & Technology in Steel Structures, Hong Kong.
[19] DIN EN 15512 (2021) *Ortsfeste Regalsysteme aus Stahl – Verstellbare Palettenregale – Grundlagen der statischen Bemessung.* Berlin: DIN Deutsches Institut für Normung e.V.
[20] EN ISO 6892-1 (2009) *Metallische Werkstoffe – Zugversuche – Teil 1: Prüfverfahren bei Raumtemperatur.* Berlin: DIN Deutsches Institut für Normung e.V.
[21] ANSYS (2020) *Version 2020 R2 [software].* ANSYS Inc. Canonsburg, Pennsylvania.
[22] Yu, W. W.; LaBoube, R.; Chen, H. (2020) *Kapitel 2 Materials used in Cold-Formed Steel Constructions.* Cold-Formed Steel Design, Ed. 5. Hoboken: Wiley.
[23] Chajes, A.; Britvec, J.; Winter, G. (1970) *Effects of cold-straining on structural sheet steels.* Effects of Work in Cold-Forming Steel Structural Members, pp. 1–36.
[24] Karren, K. W. (1970) *Corner properties of cold-formed steel shapes.* Effects of Work in Cold-Forming Steel Structural Members, pp. 55–88.
[25] Karren, K. W.; Winter, G. (1970) *Effects of cold-forming on light-gage steel members.* Effects of Work in Cold-Forming Steel Structural Members, pp. 93–131.
[26] Sloof, P. A.; Schuster, R. M. (2000) *Yield strength increase of cold formed sections due to cold work of forming.* 15th International Specialty Conference on Cold-Formed Steel Structures, pp. 517–535.
[27] Gardner, L.; Saari, N.; Wang, F. (2010) *Comparative experimental study of hot-rolled and cold-formed rectangular hollow sections.* Thin-Walled Structures 48, No. 7, pp. 527–538.
[28] Rossi, B.; Afshan, S.; Gardner, L. (2013) *Strength enhancements in cold-formed structural sections – PAT II: Predictive models.* Journal of Constructional Steel Research 83, pp. 189–196.
[29] Gardner, L.; Yun, X. (2018) *Description of stress-strain curves for cold-formed steels.* Construction and Building Material 189, pp. 527–538.
[30] Ye, J.; Hajirasouliha, I.; Becque, J. (2018) *Experimental investigation of local-flexural interactive buckling of cold formed steel channel columns.* Thin-Walled Structures 125, pp. 245–258.
[31] EN 1993-1-1/NA (2010) *Nationaler Anhang – National festgelegte Parameter. Eurocode 3: Bemessung und Konstruktion von Stahlbauten – Teil 1-1: Allgemeine Regeln und Regeln für den Hochbau.* Berlin: DIN Deutsches Institut für Normung e. V.
[32] Rasmussen, K. J. R.; Gilbert, B. P. (2013) *Analysis-based design provisions for steel storage racks.* Journal of Structural Engineering 139, No. 5, pp. 849–859.
[33] Walker, A. (1975) *Design and Analysis of Cold-Formed Sections.* London: International Textbook Company.
[34] prEN 1993-1-14 (2021) *Eurocode 3: Design of Steel Structures – Part 1-14: Design Assisted by Finite Element Analysis.* CEN/TC 250/SC 3/WG 3.
[35] Moen, C. D.; Schafer, B. W. (2010) *Direct strength method for design of cold formed steel columns with holes.* Journal of Structural Engineering 137, No. 5, pp. 559–570.
[36] Casafont, M.; Pastor, M. M.; Roure, F.; Bonada, J.; Peköz, T. (2013) *Design of steel storage rack columns via the direct strength method.* Journal of Structural Engineering 139, pp. 669–679.
[37] Cai, J.; Schafer, B. W.; Moen, C. D. (2017) *CUFSM elastic buckling analysis software module for quantifying hole effects in thin-walled structural members.* Structural Stability Research Council.

Authors

Univ.-Prof. Dr.-Ing. Dieter Ungermann
dieter.ungermann@tu-dortmund.de
TU Dortmund University
Chair of Steel Construction
August-Schmidt-Straße 6
44227 Dortmund, Germany

Tim Lemański, M.Sc. (corresponding author)
tim.lemanski@tu-dortmund.de
TU Dortmund University
Chair of Steel Construction
August-Schmidt-Straße 6
44227 Dortmund, Germany

apl. Prof. Dr.-Ing. habil. Bettina Brune
bettina.brune@tu-dortmund.de
TU Dortmund University
Chair of Steel Construction
August-Schmidt-Straße 6
44227 Dortmund, Germany

How to Cite this Paper

Ungermann, D.; Lemański, T.; Brune, B. (2023) *A Eurocode-compliant design approach for cold-formed steel sections*. Steel Construction 16, No. 2, pp. 78–92. https://doi.org/10.1002/stco.202200039

This paper has been peer reviewed. Submitted: 15. November 2022; accepted: 13. February 2023.